Seen by GSC Jan 2/81

An Experiment to Test a Source of P and S Wave Energy

by

C. Wright and P. Johnson

Seismological Service of Canada

Internal Report # 80-7

Division of Seismology

and Geothermal Studies

Earth Physics Branch

Energy, Mines & Resources Canada

October 1980

ABSTRACT

A seismic source consisting of a 700 kg weight that could be dropped vertically or projected down a ramp inclined at 45° to the vertical was tested as a source of P, SV and SH waves within a crystalline rock body at Chalk River, Ontario. The seismic energy was recorded by arrays of both horizontal and vertical-component geophones at distances between 30 and 600 m from the source, which was operated over glacial overburden varying in thickness from less than a metre to a few tens of metres. Seismic energy was more efficiently generated when the overburden thicknesses were at least several metres. The signals identified visually as S are generally true S, though some may be the converted wave (P)S. The SV amplitudes are generally larger than those of P, regardless of the type of shot, while the signal frequencies are roughly 60 Hz and 90 Hz respectively. The horizontal-component seismograms for the inclined shots showed no evidence of SH polarisation, and the SH amplitudes were only rarely enhanced relative to P and SV amplitudes on changing from vertical to inclined shots. These unexpected results are attributed to the combined effect of the high velocity and density contrasts and the irregularity of the boundary between the glacial overburden and the rock body.

INTRODUCTION

Attempts at generating and recording clearly identifiable shear waves over distance ranges from a few metres to a few kilometres have been made using explosives (Kisslinger, Mateker and McEvilly, 1961; White and Sengbush, 1963; Kitsunezaki, 1971; Dohr and Janle, 1980), specially designed shear-wave generators using explosives (Shima and Ohta, 1968; Ohta et al., 1980; R. Turpening, personal communication) and shear wave hammers or horizontal vibrators (Cherry and Waters, 1968; Kitsunezaki, 1971). There have been several motivations for this kind of work, including the study of the physics of seismic sources, the study of near-surface soils and rocks for earthquake engineering purposes and for the evaluation of construction sites, and the search for oil and natural gas. With the exception of the work of Kitsunezaki (1971), these earlier studies have been confined almost entirely to soils and sedimentary rock sequences.

The study of shear-wave propagation in crystalline rock bodies that are being tested as possible nuclear waste disposal sites may provide valuable supplementary information to P wave data for the study of the distribution of cracks, fractures and faults (Wright and Langley, 1980). A limited quantity of useful shear-wave data was obtained in October, 1977, in a gneiss-monzonite rock body at Chalk River, Ontario, using the shear-wave gun designed by R. Turpening (Lam and Wright, 1980). In this earlier experiment, the SH energy recorded showed no evidence of horizontal polarization. The Chalk River test site consists mainly of a monzonitic orthogneiss and a more mafic paragneiss, both having P wave velocities in excess of 5 km/s, covered with a thin veneer of glacial sediments with P wave velocities of about 2 km/s and thicknesses from a few centimetres to tens of metres. Surface outcrops occur in the

vicinity of Maskinonge Lake (Figure 1). Thin sheets of gabbro with P velocities of about 6.5 km/s are known to exist in some regions of the rock body (Lam and Wright, 1980). Because of similar high velocity and density contrasts at other prospective test sites that can result in extensive scattering and P to S and S to P conversions, the earlier results may indicate limitations on shear-wave studies at such sites. Clearly more work on shear wave propagation was required. Since the use of a shear-wave gun proved to be expensive, a cheaper source of S waves had to be found.

At the end of October, 1979, an experiment was undertaken at Chalk River to test a shear-wave hammer, designed and built by Mr. Earl Fulkerson of Canton, Michigan. The objectives were fourfold: (i) to determine if it is possible to generate horizontally polarised shear waves at any location on the Chalk River site, (ii) to find the distance range over which the source gives useful P and S wave energy, (iii) to compare the seismic wave amplitudes produced when the source was operated over different thicknesses of overburden, and (iv) to measure approximate P and S wave velocities within the rock body.

EXPERIMENTAL PROCEDURE

The source consisted of a 700 kg weight that could be dropped vertically on to a steel base plate firmly embedded in the glacial overburden above the rock body. To produce horizontally polarised shear waves, the weight could be made to slide down a steel 'ramp' inclined at 45° to the vertical (Figure 2). In the vertical mode of operation the weight could be dropped from a height of over 2 m; for the inclined shot positions, however, the maximum height was 0.9 m. During the experiment the weight was dropped from the right and left

inclined positions in a plane approximately at 90° to the line of the recording spread, as shown schematically in Figure 3. The weight was also dropped vertically from a height of 0.9 m to give three different types of shot at each location.

The surface recorders were deployed as shown in Figure 3 using alternating arrays of 9 vertical- and 8 horizontal-component 14 Hz geophones. The shot points were at roughly sixty-metre intervals starting 120 m from the recording truck and moving out to about 500 m. The spread was placed at the three locations shown in Figure 1. Seismograms for the shot points to the south east of the surface spread for profile 1 were also recorded by a string of twelve hydrophones suspended on a crystal cable lowered into borehole CR1. Because S waves could not be clearly identified on the hydrophones, the data recorded in the borehole will not be discussed here.

The seismic energy produced by each shot was recorded for one second at a digital rate of 2000 samples/second on twelve channels using an SIE RS-49 system. Each type of shot was produced 6 times, sometimes 10, and recorded as a single data file using the stacking capability of the system.

3. SEISMOGRAMS AND TRAVEL TIMES

General Discussion of Seismograms. The seismograms showed considerable energy over the time span expected for the S arrival, but the clear identification of the S phase on vertical- or horizontal-component instruments was sometimes difficult. Nevertheless, both P and possible S arrivals were picked by eye. For the clearest seismograms the frequencies of the P and S arrivals were typically 90 and 60 Hz respectively. At most locations, the three types of 'shot' (Figure 3) produced similar, often practically identical

seismograms. Further, the subtraction of horizontal-component seismograms produced with the weight in the right position from those produced with the weight in the left position (Figure 3) did not assist in the identification of the S wave onset. Horizontally polarised SH energy was therefore absent. A representative set of seismograms to illustrate this phenomenon is shown in Figure 4. Some of the S wave energy may be produced by conversion from P at the boundary between the overburden and the rock body immediately below the source. Such arrivals will be denoted (P)S.

Analysis of S-P versus P Times. The S-P times were plotted against the P times for all six vertical-component geophone arrays of each of the three profiles, and for each individual array of profiles 1 and 3. Because the P times contain small unknown errors that are much less than those in the S-P times, straight lines were fitted through the data sets using the maximum likelihood method of Bartlett (1949), and the results are displayed in Table 1. Figure 5 shows the results for all traces for profiles 1 and 3.

The results for the individual geophone arrays of profile 1 are rather variable, and the slopes of the lines vary between 0.69 and 0.91. A straight line through all the data has a slope of 0.749 ± 0.036 and almost zero intercept. For gneiss, the ratio of P to S velocities (α/β) is about 1.7, but for unconsolidated sediments the ratio is usually higher and may be as high as 3 or more (Ohta et al., 1980). For a shear wave, the ratio of the S to the P travel time should therefore be larger at short distances, since the fraction of the path length within the overburden is larger. Thus, the intercept on the S-P axis should generally be positive. The almost zero intercept for the complete data set therefore indicates either that α/β is close to 1.7 for the

sediments, or, alternatively, that the arrivals identified as S are really a mixture of S and (P)S.

Because of the proximity of exposed bedrock, the overburden thicknesses were believed to be less than a metre at the three shot points of profile 2 (Figure 1). A plot of S-P times against P times shows considerable scatter, caused primarily by some anomalously early low amplitude P arrivals at larger distances. Since the average velocity between source and receiver of the these early signals exceeds 6.2 km/s, the fast P times are probably due to the presence of gabbro or dolerite along much of the propagation paths.

From the results of Lam and Wright (1980), we know that the overburden below profile 3 was much thicker than that below the other two profiles. The slopes of the S-P versus P lines (Table 1) show less scatter than those of profile 1, partly because of the better signal-to-noise conditions when profile 3 was recorded; for five of the geophone arrays, the slopes lie in the range 0.67 - 0.72, but one yields an anomalously low slope of 0.47. The slope for all geophone arrays is 0.679 ± 0.040, which is significantly lower than the corresponding result for profile 1. The intercept with the S-P axis is positive, but differs from zero by little more than its standard deviation; the picked S arrivals therefore seem to be again a mixture of true S and (P)S.

Analysis of Travel Times as a Function of Distance. For profile 1, the P and S travel times as a function of distance were split into two groups: one for shot points 1-5 to the south east and the other for shot points 6 - 11 to the north west of the geophone spread. They were further subdivided into three subsets for P waves, consisting of times at adjacent pairs of vertical-component geophone arrays, and into six subsets for S waves

consisting of times at adjacent pairs of horizontal-component as well as vertical-component geophone arrays. A straight line was fitted through the data for each subset, again using the maximum likelihood method of Bartlett (1949), and the results are summarised in Tables 2 and 3 for P and S waves respectively. These lines provide apparent velocities (reciprocal slopes) of the signals averaged over the two areas spanned by shot points 1-5 and 6-11 (Figure 1).

For shot points 1-5, the apparent velocities of P and S cover the ranges 5.22 - 5.51 km/s and 2.80 - 3.11 km/s respectively. The comparatively large standard errors on the P velocities are not due to errors in the time picks, but are due to the inhomogeneity of the structure along the profiles. From the results of Mair and Lam (1979) and Wright, Johnston and Lam (1980), there is apparently no significant increase or decrease in the thickness of overburden between shot points 1 and 5, but the velocities in the underlying gneiss tend to decrease towards the south east. The average P velocities in the gneiss between these shot points, calculated from each of the two sets of data presented by Wright et al. (1980), are 5.34 and 5.42 km/s. The calculated apparent velocities therefore seem to be reliable indicators of the true P and S wave velocities within the rock body.

The results of Mair and Lam (1979) and Wright et al. (1980) also indicate no large changes in thickness or velocity below shot points 6-11, and data from Wright et al. yield an average P velocity in the gneiss of 5.53 km/s. The apparent velocities of P and S waves generated at these shot points are comparatively high, lying in the range 6.30 - 6.38 km/s and 3.44 -3.99 km/s respectively. We suggest that the lower P velocities derived by Wright et al. (1980) over the same region occur because of the comparative shortness of the

profiles (maximum shot-geophone distance = 240 m), and are influenced only by the top 20 m or so of the rock body. The higher apparent velocities for the longer profile may be due to propagation within an almost horizontal, high velocity wave-guide (probably gabbro) about 30 m below the surface along part of the propagation paths; the results for the adjacent profile 2 support this interpretation.

Profile 2 samples a region adjacent to the higher velocity portion of profile 1, and the apparent velocities of S (Table 3) show good agreement with the corresponding S velocities for profile 1. The apparent velocity of P (Table 2) is high and poorly defined because of the presence of a few anomalously early P arrivals at large distances. This phenomenon is attributed to the presence of gabbro beneath part of the profile.

The time-distance data for profile 3 can only be crudely represented by a straight line. Comparatively large errors in apparent velocities for P are consequently due to real complexity of structure rather than errors in time measurements (Table 2). The apparent velocities for P and S (Tables 2 and 3) lie in the range 7.17 to 7.56 km/s and 4.14 to 4.78 km/s respectively, and the high intercepts compared with profiles 1 and 2 indicate a considerable thickness of sediments. Lam and Wright (1980) suggested that a thin, almost horizontal sheet of gabbro with P and S wave velocities of 6.56 and 4.09 km/s lies beneath the recording spread of profile 3 and extends south west almost to borehole CR1. If we assume that the true P wave velocity is 6.56 km/s, the S velocity becomes 3.92 km/s.

Other Features of Seismograms. A search for systematic differences between SH and SV arrival times was unsuccessful. Thus, to the accuracy

obtainable in the experiment ($\sim$3% in S times), SH and SV velocities are the same. Even though we sought to generate SH waves, clear S wave arrivals were more frequently observed on the vertical-component instruments. Some relevant statistics for profile 3 are listed in Table 4, where clear S arrivals on vertical- and horizontal-component instruments were observed for 64.6% and 41.7% of seismograms respectively. The high velocity and density contrasts at the boundary and the irregularity of the contact between the overburden and the rock body are largely responsible for the absence of horizontally polarised S waves. The comparative lack of rigidity of the overburden, particularly for profiles 1 and 2, may also be a contributing factor, resulting in the generation of (P)S in place of S.

4. AMPLITUDES

Amplitude-Distance Data. For all vertical-component seismograms, the peak-to-peak amplitudes of both the wave train between P and S or (P)S and the first cycle of the S or (P)S wave train were measured. However, only the peak-to-peak amplitudes of the first cycle of the S or (P)S wave train were measured on the horizontal-component instruments. The amplitudes were expressed in arbitrary units, taking the P amplitude at vertical array 9 from the first shot point of profile 1 as 1000 units. For each shot-recorder path, the average of the logarithm of the amplitudes of each of the three types of shot was determined. The curvature of each plot of the logarithm of the amplitude (A) versus distance (Δ) indicated that a power law of amplitude decay of the form $A = C\Delta^{-n}$ was a better approximation to the data than an exponential law. Therefore, to determine the exponents, a linear regression of log (amplitude) upon log (distance) was undertaken for both P and S data.

The results and the manner in which the data were subdivided are shown in Table 5, and the fitted log (amplitude) versus distance curves are plotted in Figure 6. We did not work with log (amplitude/period) because the observed change of period from the closest to the most distant geophones was small (<20%).

Profile 1 (Figure 1). The data recorded to the south east (shot points 1-5) and to the north west (shot points 6-11) were analysed separately. The decay of amplitude as a function of distance for shot points 1-5 is very slow, the exponent n being 0.37 for P and 0.59 and 0.48 for SV and SH respectively. There is some evidence, therefore, that any anelastic attenuation of S is slightly larger than that for P, while the amplitudes for both P and S decay approximately as the square root of the distance. For shot points 6-11, the amplitudes for both P and S decay more rapidly, the exponents being 0.79 for P, and 1.74 and 1.03 for SV and SH respectively.

Profile 2 (Figure 1). The limited and fairly poor quality amplitude data for profile 2 show a more rapid decay as a function of distance than the data for profile 1. The exponent for P is 1.54 and the corresponding exponents for SV and SH are 2.09 and 1.07 respectively. As for profile 1, the SV amplitudes decay much more rapidly as a function of distance than the SH amplitudes.

Profile 3 (Figure 1). This profile was recorded over a greater thickness of overburden than the other two profiles (Tables 2 and 3). The P travel times are early for geophone arrays 7-11, relative to those for arrays 1-5 (Table 2), suggesting different structures below the two halves of the

recording spread. For this reason, the amplitude data for the two halves of the spread were treated separately, and the data and regression lines are plotted in Figures 7-9.

In comparison with profiles 1 and 2, the amplitudes are larger at short distances, but decay much more rapidly with distance, and the results for P, SV and SH are very similar. Vertical-component geophone arrays 7, 9 and 11 record P and SV amplitudes roughly twice as large as arrays 1, 3 and 5. A similar phenomenon occurs for the horizontal-component geophone arrays 8, 10 and 12, which record amplitudes slightly less than double those of arrays 2, 4 and 6. The S wave amplitudes may decay slightly faster than the P amplitudes, possibly because of greater anelastic attenuation of S; the exponents (Table 5) are 1.77 and 1.75 for P, 1.72 and 2.22 for SV and 1.91 and 2.13 for SH. The S amplitudes therefore obey an inverse square law of decay to a good approximation, with the corresponding P amplitudes decaying a little slower. Note the marked contrast to profiles 1 and 2 where the SV amplitudes dropped more rapidly than the P or SH amplitudes.

Comparison of Profiles. The slower amplitude decay rates for profiles 1 and 2 relative to profile 3 are attributed to three main causes: more extensive scattering and P to S and S to P conversions due to the inhomogeneity of the overburden and the irregularity of the boundary between overburden and the underlying rock body, more extensive weathering and alteration of the top few metres of the rock body, and relatively high noise level during recording.

Amplitude Ratios. In an attempt to explain the absence of S wave polarisation, further analysis of the amplitudes of the signals was

undertaken. Initially, amplitude ratios A_{SV}/A_P were plotted as a function of distance for profile 3, as shown in Figure 10. The superimposed histogram was constructed from the average of the logarithms of the amplitude ratios in each cell. A histogram of the 46 values of $\log_{10}(A_{SV}/A_P)$ is inset on the right of the diagram, together with a normal distribution curve having the same mean and standard deviation. The amplitude ratios thus conform approximately to a lognormal distribution. The most probable value of the amplitude ratio is therefore the geometric mean, which is 1.77. The amplitude ratios seem to decrease slowly with increasing distance between 100m and 600m from the source. Between 30m and 100m, however, the ratios appear to increase with increasing distance; this effect is possibly an artifact caused by the proximity of the P and S arrivals, resulting in complex interference effects between the two wave groups. The weight drop source therefore generates SV waves with amplitudes larger than those of P waves, regardless of whether it is operated in the vertical or slanted positions.

In Figures 11 and 12, the amplitude ratios for the right and left slanted shots relative to the vertical shots are plotted for each geophone array and each source location for profile 3. Figure 11 shows the results for geophone arrays 1-6. For both P and SV, the amplitude ratios show similar variations within the range 0.30 to 0.96, the left slanted shots tending to have higher amplitudes than the right shots. Only shot points 5, 6 and 7 yielded amplitude ratios greater than one, and only one shot point resulted in consistently higher amplitudes for all three horizontal-component geophone arrays. An unexpected result thus emerges; the slanted shots only rarely generate higher SH amplitudes than the vertical shots.

Figure 12 shows the results for geophone arrays 7-12. The P and SV amplitude ratios are often close to, and occasionally greater than unity.

Further, the SH amplitude ratios do not appear to be significantly larger than those of P or SV, and the tendency for the left shot to produce larger amplitudes has disappeared. The foregoing results may possibly be due to misalignment by more than 10° of the plane of the slanted shots relative to the line of geophone arrays. The winding access road along profile 3 and the soft, sandy terrain made it difficult in some instances to align the source accurately. However, similar amplitude ratios for profiles 1 and 2 are rather scattered and do not indicate preferential SH generation or SH polarisation, even though the source was generally more accurately aligned relative to the horizontal geophone arrays. The results suggest that local inhomogeneities dominate the radiation of P and S wave energy, irrespective of the thickness of sediments, and the orientation of the source has little effect on the relative amounts of P, SV and SH energy generated.

5. DISCUSSION AND CONCLUSIONS

The comparatively large formal errors in the P wave velocities of Table 2 are due to real deviations from linearity in the time-distance data, and are not due to uncertainties in picking the first breaks. The lower errors for the S wave data of Table 3 are partly due to the use of both SV and SH data, thus giving approximately twice as many observations of S as P. However, the travel time-distance data for S also show less scatter about the maximum likelihood lines than the P data. This effect may be an artifact introduced by the observer in the subjective process of picking the S arrival times; alternatively, it may be a real phenomenon caused by varying saturation conditions in the glacial overburden, which will cause subtle variations in P travel times but no corresponding variations in S travel times.

In spite of the absence of SH polarisation, S wave velocities of 2.90 ± 0.05, 3.73 ± 0.10 and 3.92 ± 0.06 km/s were obtained within the rock body along three different paths with corresponding P velocities of 5.26 ± 0.12, 6.35 ± 0.17 and 6.56 ± 0.17 km/s. The absence of SH polarisation on the horizontal-component instruments is an enigma, but does not appear to be the result of a technical deficiency in the source; it is most probably due to the complexity of the boundary and the large changes of elastic parameters between the overburden and the rock body. It appears, therefore, that the environment itself is more of a problem than the choice of seismic source.

Some excellent examples of SH polarisation from the weight drop source were obtained in the Michigan Basin, using a three-component lock-in geophone placed in a borehole (R. Stewart, personal communication); the source was used above sedimentary rocks with less extreme velocity and density contrasts, and the experiment has been described briefly by Stewart, Toksöz and Turpening (1980).

Plans for future experiments involve recording in a borehole with a three-component lock-in type of transducer. SH polarisation may be more readily observable under these conditions, because the seismic energy has to traverse the irregular sediment-rock body interface only once. At Chalk River the effective distance range over which the inclined source can be used is at least 600m. From the earlier work of Lam and Wright (1980), this range can be increased to about 1.3 km for the vertical shots when the maximum height is used. An experiment was completed at Pinawa, Manitoba, in September, 1980, using the hammer source and conventional explosives. The granite rock body and its contact with the overlying sediments are believed to be more uniform compared with the Chalk River site. The presence or absence of polarised SH waves, both on the surface and in a borehole, will tell us whether there are limitations on S wave studies at potential disposal sites.

ACKNOWLEDGEMENTS

We wish to thank Drs. G.G.R. Buchbinder and J.A. Mair for critically reading an earlier draft of this manuscript. We also wish to thank Dr. J.A.M. Hunter of the Geological Survey of Canada for the loan of the seismic recording equipment used in the experiment. We gratefully acknowledge the assistance of Mr. Earl Fulkerson and several members of staff of the Earth Physics Branch and the Geological Survey of Canada with field operations.

REFERENCES

BARTLETT, M.S., 1949,
Fitting a straight line when both variables are subject to error, Biometrics, 5, 207-212.

CHERRY, J.T., and WATERS, K.H., 1968,
Shear-wave recording using continuous signal methods: part 1 - early development, Geophysics, 33, 229-239.

DOHR, G., and JANLE, H., 1980,
Improvements in the observation of shear waves, Geophys. Prosp., 28, 208-220.

KISSLINGER, C., MATEKER, E.J., and McEVILLY, T.V., 1961,
SH motion from explosions in soils, J. Geophys. Res., 66, 3487-3496.

KITSUNEZAKI, C., 1971,
Field-experimental study of shear waves and the related problems, Contributions, Geophys, Inst., Kyoto Univ., 11, 103-177.

LAM, C.P., and WRIGHT, C., 1980,
Seismic wave velocities in a rock body at Chalk River, Ontario: part 1, Atomic Energy of Canada Limited Report, TR 40-1, 36 pp., Pinawa, Manitoba.

MAIR, J.A., and LAM, C.P., 1979,
High resolution seismic profiling, Chalk River, Atomic Energy of Canada Limited Report RW/GPH, 79-009, 7 pp., Pinawa, Manitoba.

OHTA, Y., GOTO, N., YAMAMIZU, F., and TAKAHASHI, H., 1980,
S-wave velocity measurements in deep soil deposit and bedrock by means of an elaborated down-hole method, Bull. Seismol. Soc. Am., 70, 363-377.

SHIMA, E., and OHTA, Y., 1968,
Experimental study on generation and propagation of S waves I: Designing SH wave generator and its field tests, Bull. Earthquake Res. Inst. Tokyo Univ., 45, 19-31.

STEWART, R.R., TOKSÖZ, M.N., and TURPENING, R., 1980,
Study of a subsurface fracture zone by vertical seismic profiling, EOS, Trans. Am. Geophys. Union 60, No. 17, (abstract) 308.

WHITE, J.E., and SENGBUSH, R.L., 1963,
Shear waves from explosive sources, Geophysics, 28, 1001-1019.

WRIGHT, C., and LANGLEY, K., 1980,
Estimates of crack density parameters in near-surface rocks from laboratory studies of core samples and in-situ seismic velocity measurements, Atomic Energy of Canada Limited Report TR 33, 19 pp., Pinawa, Manitoba.

WRIGHT, C., JOHNSTON, M., and LAM, C.P., 1980,
Seismic wave velocities in a rock body at Chalk River, Ontario: part 2,
Atomic Energy of Canada Limited Report, TR 40-2, 12 pp.

FIGURE CAPTIONS

Figure 1: Map of the Chalk River site showing the deployment of source and geophones. The sediment cover becomes thicker towards the north east. T_1, T_2 and T_3 denote the extent of the three positions of the geophone spread. For position T_3, only shot points 11, 12 and 13 were used.

Figure 2: The modified hammer used as a shear wave source. The weight is resting on the base plate, while the steel 'ramp' is moving from the vertical towards the inclined position used for SH generation.

Figure 3: Schematic diagram showing source-geophone configuration.

Figure 4: A set of seismograms to illustrate the similarity of the signal produced for the vertical, right and left positions of the weight. Profile 3: distances to nearest and farthest geophone arrays are 203.7 m and 339.3 m respectively. P and S arrivals are marked by a vertical bar. S arrivals on channels 4, 10, 11 and 12 are not clear.

Figure 5: S-P times plotted against P times for all geophones of (a) profile 1 and (b) profile 3. The lines through the data were fitted by the maximum likelihood method of Bartlett (1949).

Figure 6: Fitted $\log_{10}$ (amplitude) versus distance curves for profiles 1, 2 and 3.

Figure 7: Log_{10} (amplitude) versus log_{10} (distance) and regression lines for P data of profile 3.

Figure 8: Log_{10} (amplitude) versus log_{10} (distance) and regression lines for SV data of profile 3.

Figure 9: Log_{10} (amplitude) versus log_{10} (distance) and regression lines for SH data of profile 3.

Figure 10: Amplitude Ratios (A_{SV}/A_P) plotted as a function of distance for profile 3.

Figure 11: Amplitude Ratios A_R/A_V, A_L/A_V for geophone arrays 1-6, profile 3. A_R, A_L and A_V are the amplitudes for the right, left and vertical shots respectively.

Figure 12: Amplitude Ratios A_R/A_V, A_L/A_V for geophone arrays 7-12, profile 3. A_R, A_L and A_V are the amplitudes for the right, left and vertical shots respectively.

Table 1: Summary of S-P versus P Data for All Profiles.

(Line Fit by Maximum Likelihood Method of Bartlett (1949))

	Slope of Line	Intercept on S-P Axis, (ms)	No. of Degrees of Freedom	
Individual geophone arrays	Between 0.69 and 0.91	Between -11.4 and 2.3	-	Profile 1
All geophones	0.749 ± 0.036	0.13 ± 2.12	53	
All geophones	0.608 ± 0.147	9.67 ± 5.16	6*	Profile 2
Individual geophone arrays	Between 0.47 and 0.72	Between -3.1 and 24.4	-	Profile 3
All geophones	0.679 ± 0.040	4.43 ± 3.46	45	

*Data from anomalously early P arrivals were not included

Table 2: Summary of P Times versus Distance (Δ) for all Profiles.

(Line Fit by Maximum Likelihood Method of Bartlett (1949))

Geophone Array Nos.	Intercept (ms)	No. of Degrees of Freedom	Apparent Velocity, (km/s)	Shot Nos.	
1,3	7.81 ± 1.72	8	5.25 ± 0.26	1-5	
5,7	8.20 ± 1.27	8	5.22 ± 0.15	1-5	Profile 1 (south east)
9,11	9.46 ± 3.50	7	5.51 ± 0.36	1-5	
		Weighted mean	5.257 ± 0.120		
1,3	18.60 ± 2.67	5	6.30 ± 0.33	6-11	
5,7	17.08 ± 2.06	7	6.37 ± 0.25	6-11	Profile 1 (north west)
9,11	16.52 ± 2.23	10	6.38 ± 0.37	6-11	
		Weighted mean	6.351 ± 0.173		
2,4,6, 7,9,11	14.78 ± 3.68	10	8.76 ± 1.32	11-13	Profile 2
1	45.21 ± 2.08	6	7.56 ± 0.44	1-9	
3	44.34 ± 2.19	6	7.41 ± 0.41	1-9	
5	42.55 ± 2.60	6	7.24 ± 0.43	1-9	
7	35.99 ± 2.48	6	7.17 ± 0.36	1-9	Profile 3
9	39.37 ± 3.05	6	7.26 ± 0.43	1-9	
11	41.72 ± 3.70	6	7.25 ± 0.48	1-9	
		Weighted mean	7.310 ± 0.172		

Table 3: Summary of S Times versus Distance (Δ) for all Profiles.

(Line Fit by Maximum Likelihood Method of Bartlett (1949))

Geophone Array Nos. and Wave Type	Intercept (ms)	No. of Degrees of Freedom	Apparent Velocity, (km/s)	Shot Nos.	
1,3 SV	11.70 ± 1.95	8	2.80 ± 0.08	1-5	
2,4 SH	14.11 ± 2.19	7	2.91 ± 0.10	1-5	
5,7 SV	11.71 ± 3.29	8	2.92 ± 0.12	1-5	Profile 1
6,8 SH	13.65 ± 3.92	8	2.97 ± 0.14	1-5	(south east)
9,11 SV	16.81 ± 6.65	7	3.11 ± 0.22	1-5	
10,12 SH	14.59 ± 7.09	8	3.11 ± 0.22	1-5	
		Weighted mean	2.900 ± 0.049		
1,3 SV	39.09 ± 4.94	5	3.99 ± 0.24	6-11	
2,4 SH	38.49 ± 6.17	5	3.95 ± 0.31	6-11	
5,7 SV	25.57 ± 6.32	7	3.44 ± 0.22	6-11	Profile 1
6,8 SH	33.58 ± 3.55	9	3.73 ± 0.18	6-11	(north west)
9,11 SV	27.69 ± 4.48	10	3.60 ± 0.23	6-11	
10,12 SH	23.59 ± 4.66	9	3.88 ± 0.33	6-11	
		Weighted mean	3.729 ± 0.097		
2,4,6,7, 9,11, SV	20.31 ± 3.49	15	3.76 ± 0.20	11-13	Profile 2
1,3,5,8, 10,12 SH	17.56 ± 2.61	16	3.62 ± 0.14	11-13	
		Weighted mean	3.664 ± 0.112		
1 SV	74.35 ± 2.75	6	4.38 ± 0.19	1-9	
2 SH	77.73 ± 2.94	6	4.55 ± 0.22	1-9	
3 SV	75.23 ± 2.80	6	4.30 ± 0.18	1-9	
4 SH	75.17 ± 3.62	6	4.30 ± 0.22	1-9	
5 SV	72.72 ± 2.48	6	4.14 ± 0.13	1-9	
6 SH	75.04 ± 3.31	6	4.31 ± 0.19	1-9	
7 SV	69.40 ± 5.17	6	4.20 ± 0.26	1-9	Profile 3
8 SH	73.25 ± 5.03	6	4.51 ± 0.28	1-9	
9 SV	72.22 ± 4.88	6	4.33 ± 0.24	1-9	
10 SH	77.97 ± 4.34	6	4.58 ± 0.23	1-9	
11 SV	79.39 ± 4.20	6	4.64 ± 0.22	1-9	
12 SH	80.47 ± 5.61	6	4.78 ± 0.31	1-9	
		Weighted mean	4.364 ± 0.060		

Table 4: Statistics on S Wave Arrivals for Profile 3

Geophone Array No. and Type	No. of Clear S Wave Arrivals	Total No. of S Wave Arrivals
1V	8	8
2H	3	8
3V	6	8
4H	5	8
5V	5	8
6H	3	8
7V	6	8
8H	2	8
9V	5	8
10H	4	8
11V	1	8
12H	3	8
All Vertical - Component Phones	31 (64.6%)	48
All Horizontal - Component Phones	20 (41.7%)	48

Table 5: Curve Fitting Results for Amplitude (A) versus Distance (Δ) Data.

A line of the form $\log_{10}(A/A_o) = -n\log_{10}\Delta + K$ was fitted to each data set by regression of $\log_{10}(A/A_o)$ upon $\log_{10}\Delta$. A_o is the reference amplitude defined in the text, and n and K are constants.

Data Set and Profile Nos.	Shot Point Nos.	Geophone Array Nos.	Wave Type	Exponent, n
1, 1	1-5	1,3,5,7,9,11	P	0.37 ± 0.16
2, 1	1-5	1,3,5,7,9,11	SV	0.59 ± 0.12
3, 1	1-5	2,4,6,8,10,12	SH	0.48 ± 0.17
4, 1	6-11	1,3,5,7,9,11	P	0.79 ± 0.19
5, 1	6-11	1,3,5,7,9,11	SV	1.74 ± 0.18
6, 1	6-11	2,4,6,8,10,12	SH	1.03 ± 0.16
7, 2	11-13	2,4,6,7,9,11	P	1.54 ± 0.28
8, 2	11-13	2,4,6,7,9,11	SV	2.09 ± 0.30
9, 2	11-13	1,3,5,8,10,12	SH	1.07 ± 0.47
10, 3	1-9	1,3,5	P	1.77 ± 0.09
11, 3	1-9	1,3,5	SV	1.72 ± 0.11
12, 3	1-9	2,4,6	SH	1.91 ± 0.20
13, 3	1-9	7,9,11	P	1.75 ± 0.22
14, 3	1-9	7,9,11	SV	2.22 ± 0.22
15, 3	1-9	8,10,12	SH	2.13 ± 0.22

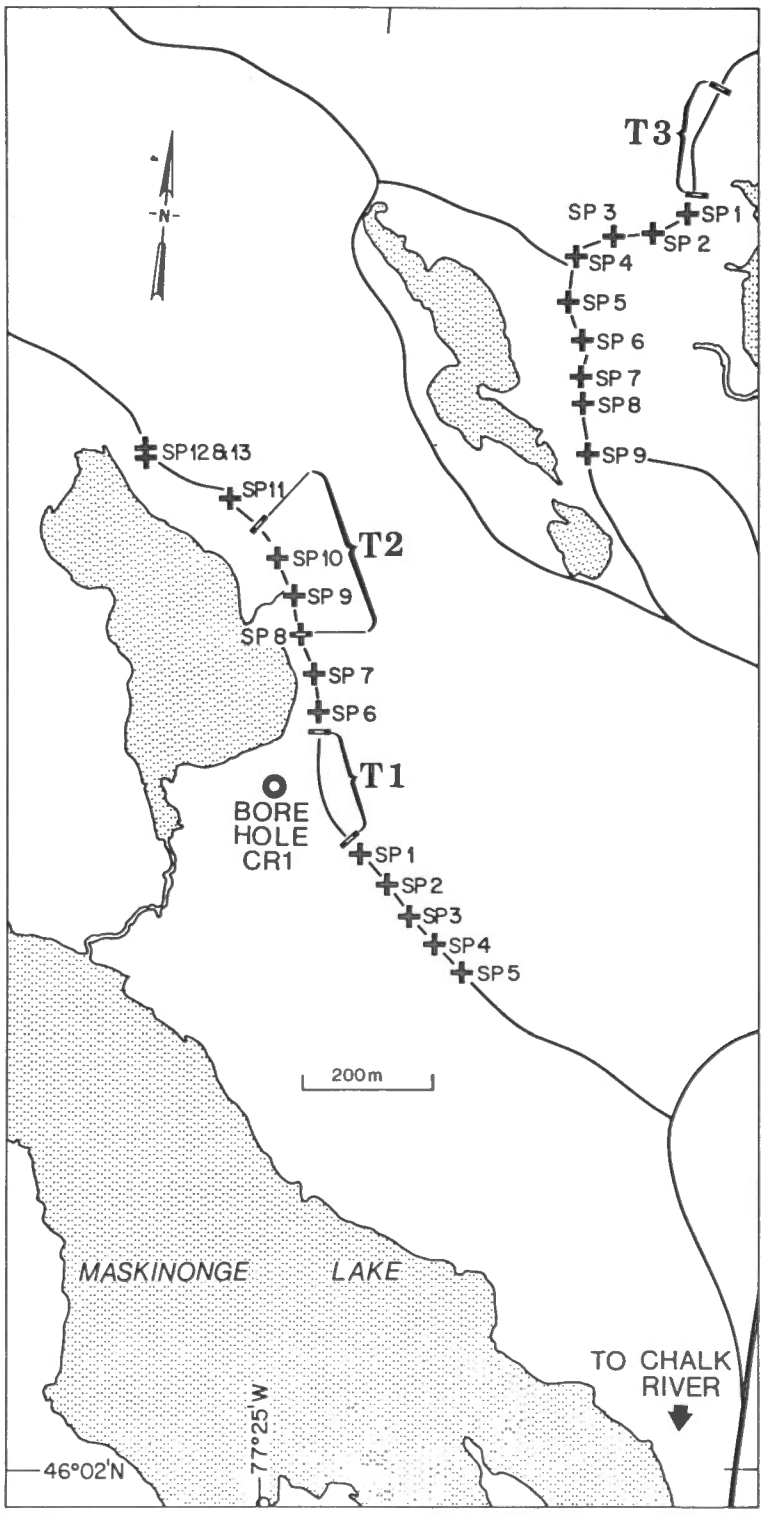
T3
SP 3
SP 1
SP 2
SP 4
SP 5
SP 6
SP 7
SP 8
SP 9
SP12&13
SP11
T2
SP10
SP 9
SP 8
SP 7
SP 6
T1
BORE
HOLE
CR1
SP 1
SP 2
SP 3
SP 4
SP 5
200m
MASKINONGE
LAKE
TO CHALK
RIVER
46°02'N
77°25'W

FIG. 1

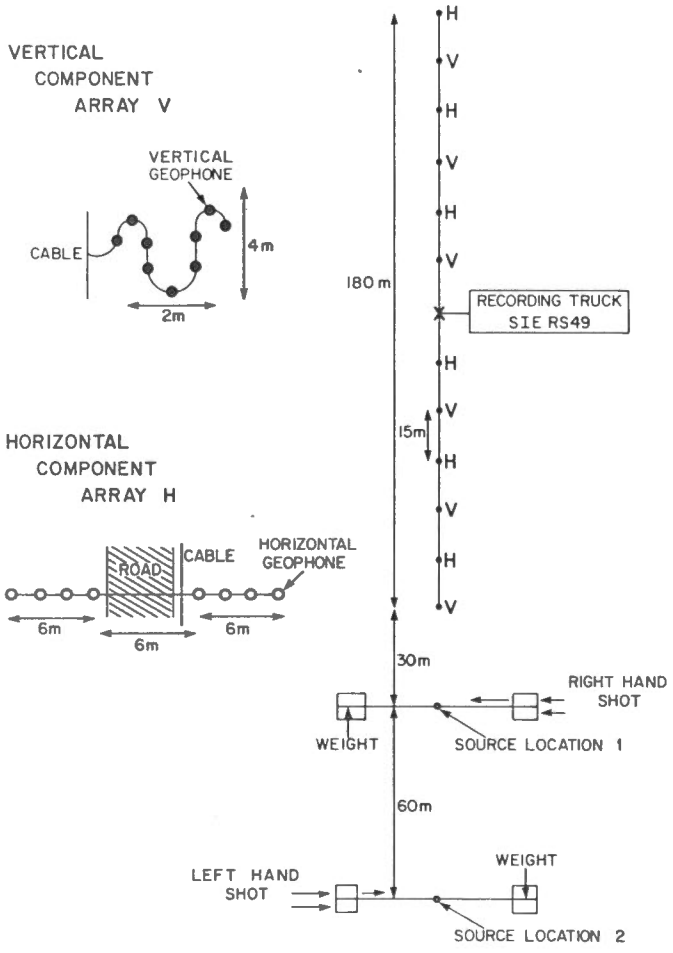
VERTICAL
COMPONENT
ARRAY V
VERTICAL
GEOPHONE
CABLE
4m
2m
HORIZONTAL
COMPONENT
ARRAY H
ROAD
CABLE
HORIZONTAL
GEOPHONE
6m
6m
6m
H
V
H
V
H
V
180 m
RECORDING TRUCK
SIE RS49
H
V
15m
H
V
H
V
30m
RIGHT HAND
SHOT
WEIGHT
SOURCE LOCATION 1
60m
WEIGHT
LEFT HAND
SHOT
SOURCE LOCATION 2

FIG. 3

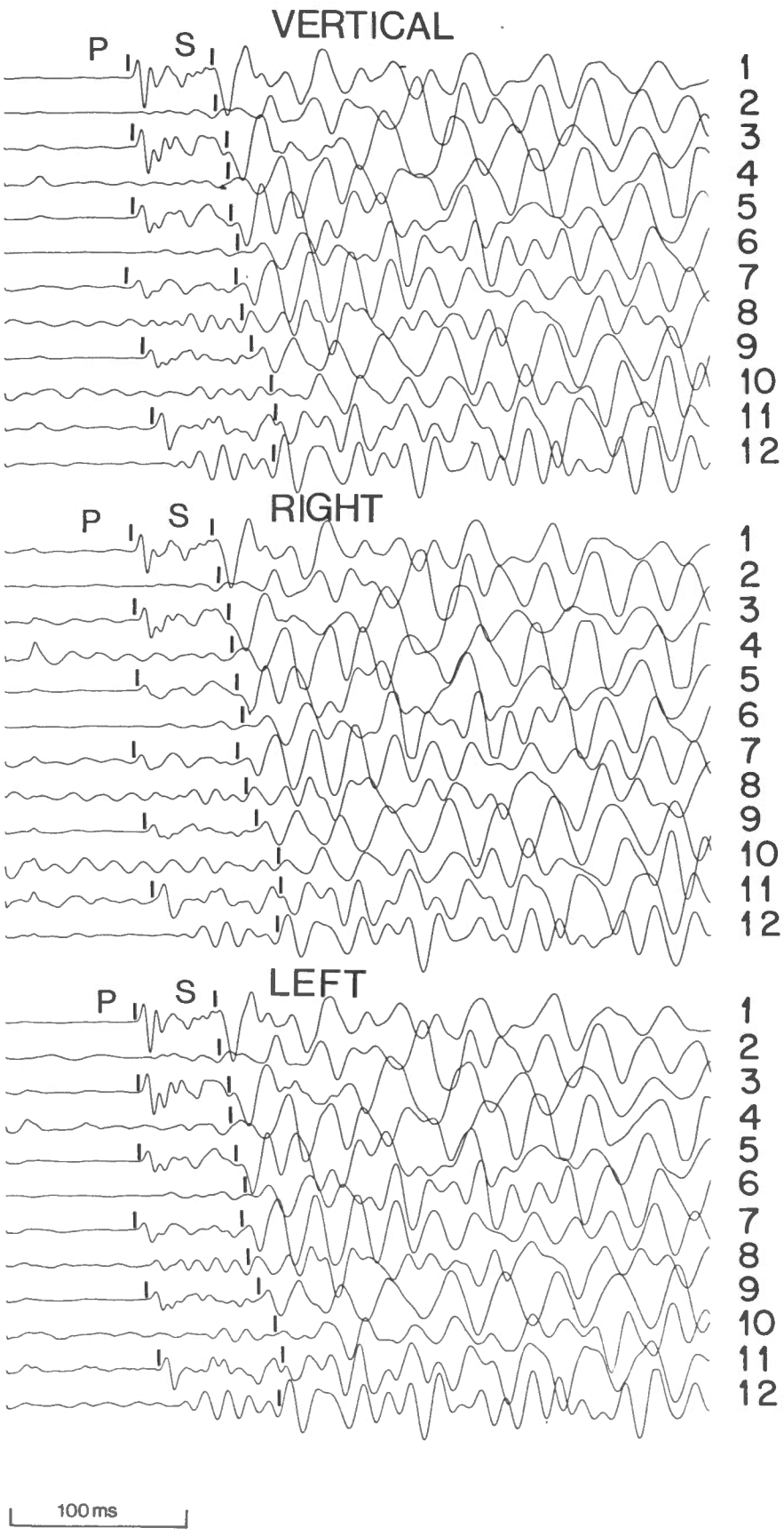
VERTICAL
P
S
1
2
3
4
5
6
7
8
9
10
11
12
RIGHT
P
S
1
2
3
4
5
6
7
8
9
10
11
12
LEFT
P
S
1
2
3
4
5
6
7
8
9
10
11
12
100 ms

FIG. 4

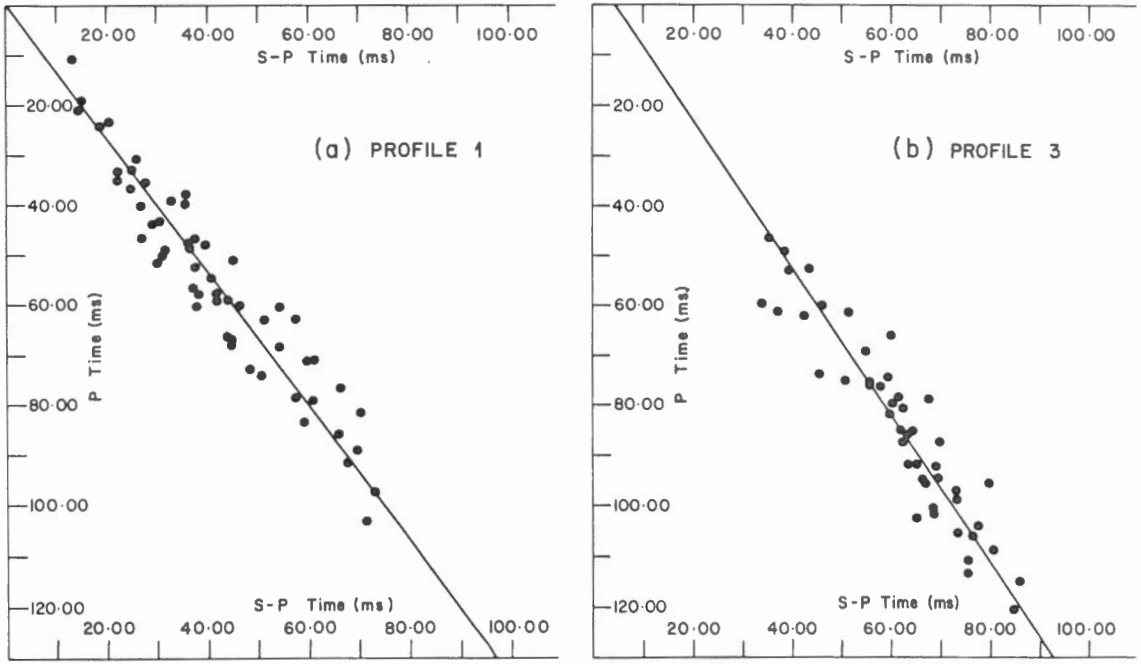
20·00
40·00
60·00
80·00
100·00
S-P Time (ms)
(a) PROFILE 1
(b) PROFILE 3
P Time (ms)
120·00

FIG. 5

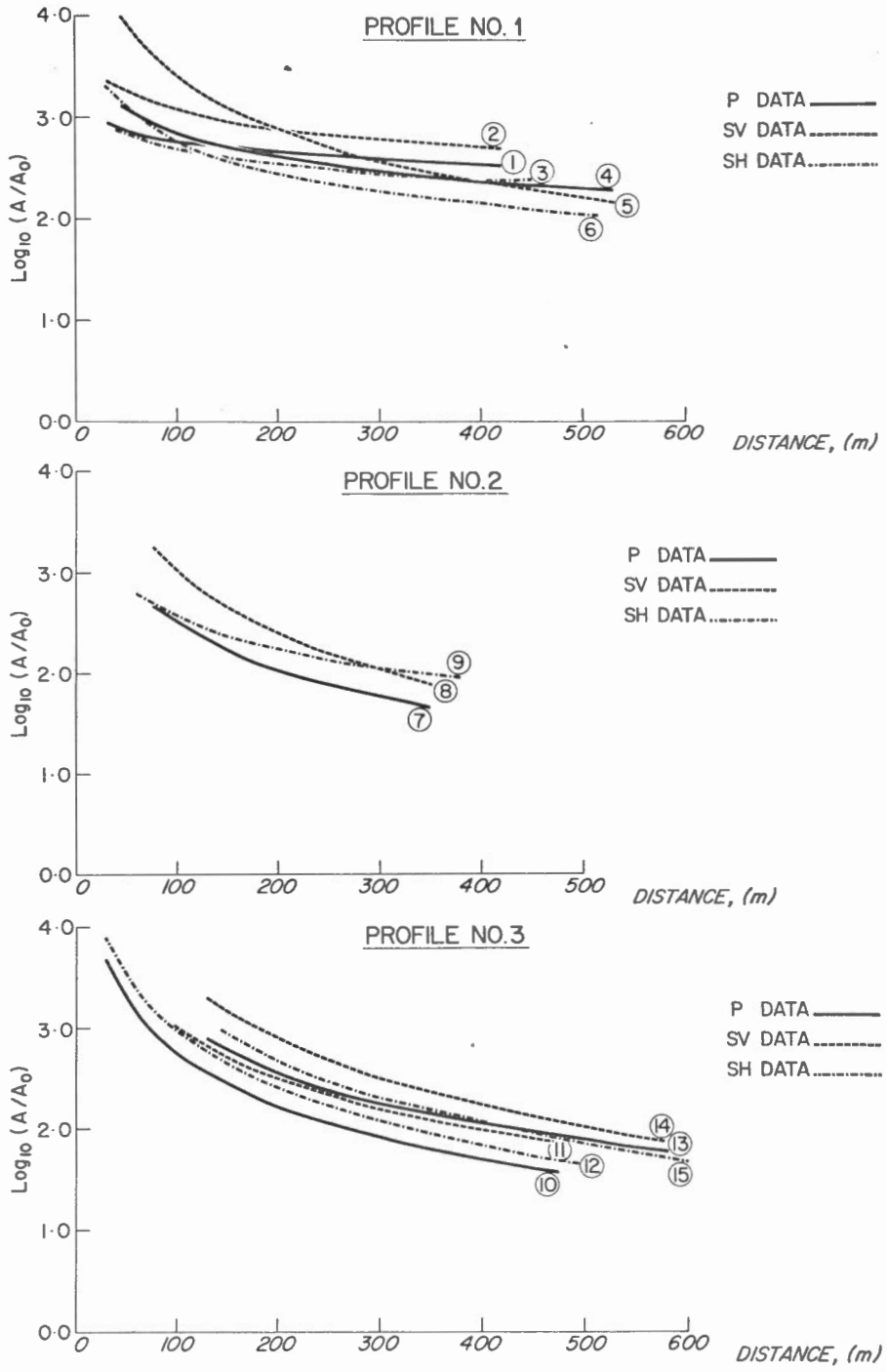
PROFILE NO. 1
P DATA
SV DATA
SH DATA
Log10 (A/A0)
4·0
3·0
2·0
1·0
0·0
0
100
200
300
400
500
600
DISTANCE, (m)
①
②
③
④
⑤
⑥
PROFILE NO.2
P DATA
SV DATA
SH DATA
Log10 (A/A0)
4·0
3·0
2·0
1·0
0·0
0
100
200
300
400
500
DISTANCE, (m)
⑦
⑧
⑨
PROFILE NO.3
P DATA
SV DATA
SH DATA
Log10 (A/A0)
4·0
3·0
2·0
1·0
0·0
0
100
200
300
400
500
600
DISTANCE, (m)
⑩
⑪
⑫
⑬
⑭
⑮

FIG. 6

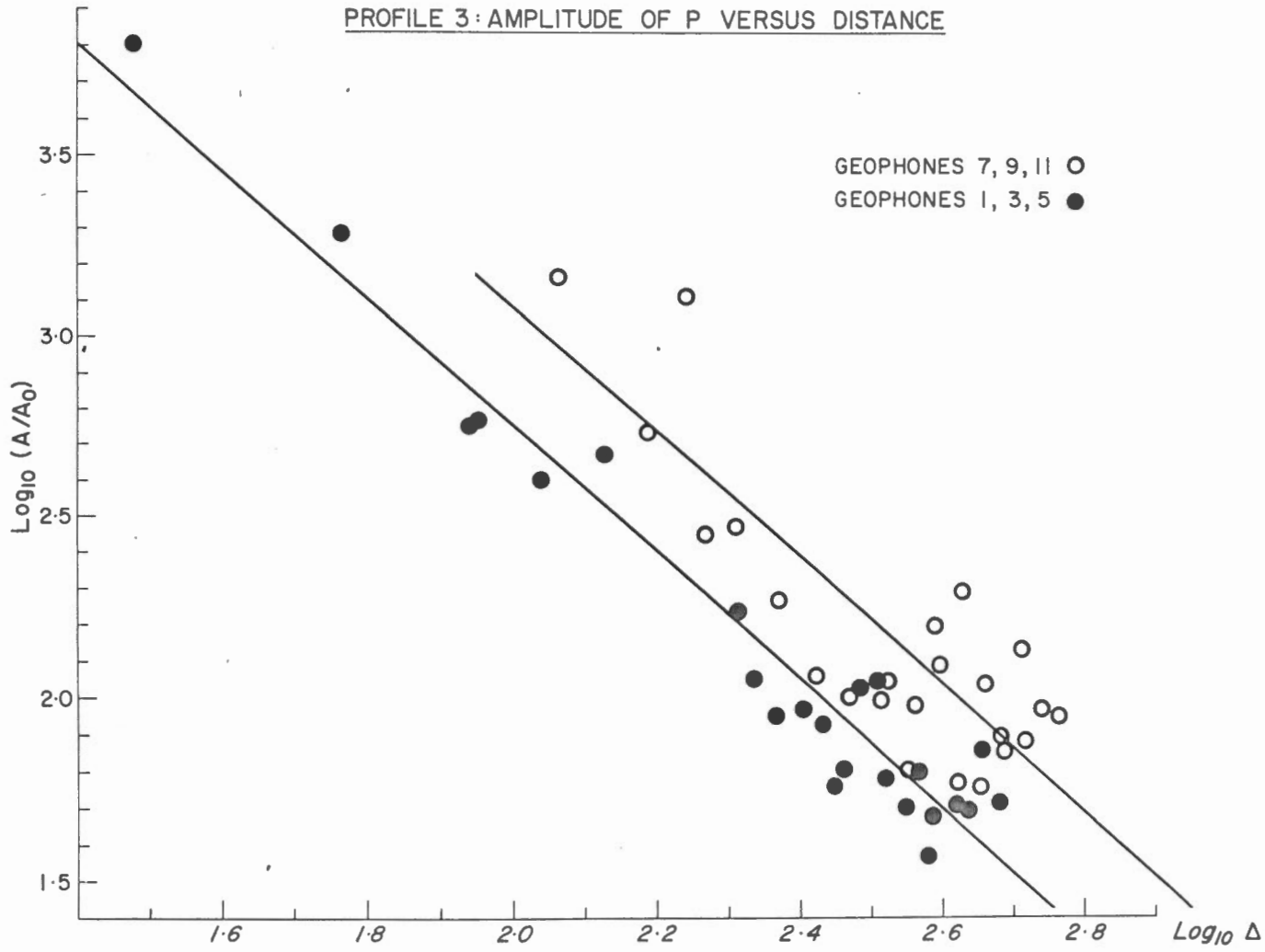
PROFILE 3 : AMPLITUDE OF P VERSUS DISTANCE
GEOPHONES 7, 9, 11
GEOPHONES 1, 3, 5
3·5
3·0
2·5
2·0
1·5
Log10 (A/A0)
1·6
1·8
2·0
2·2
2·4
2·6
2·8
Log10 Δ

Fig. 7

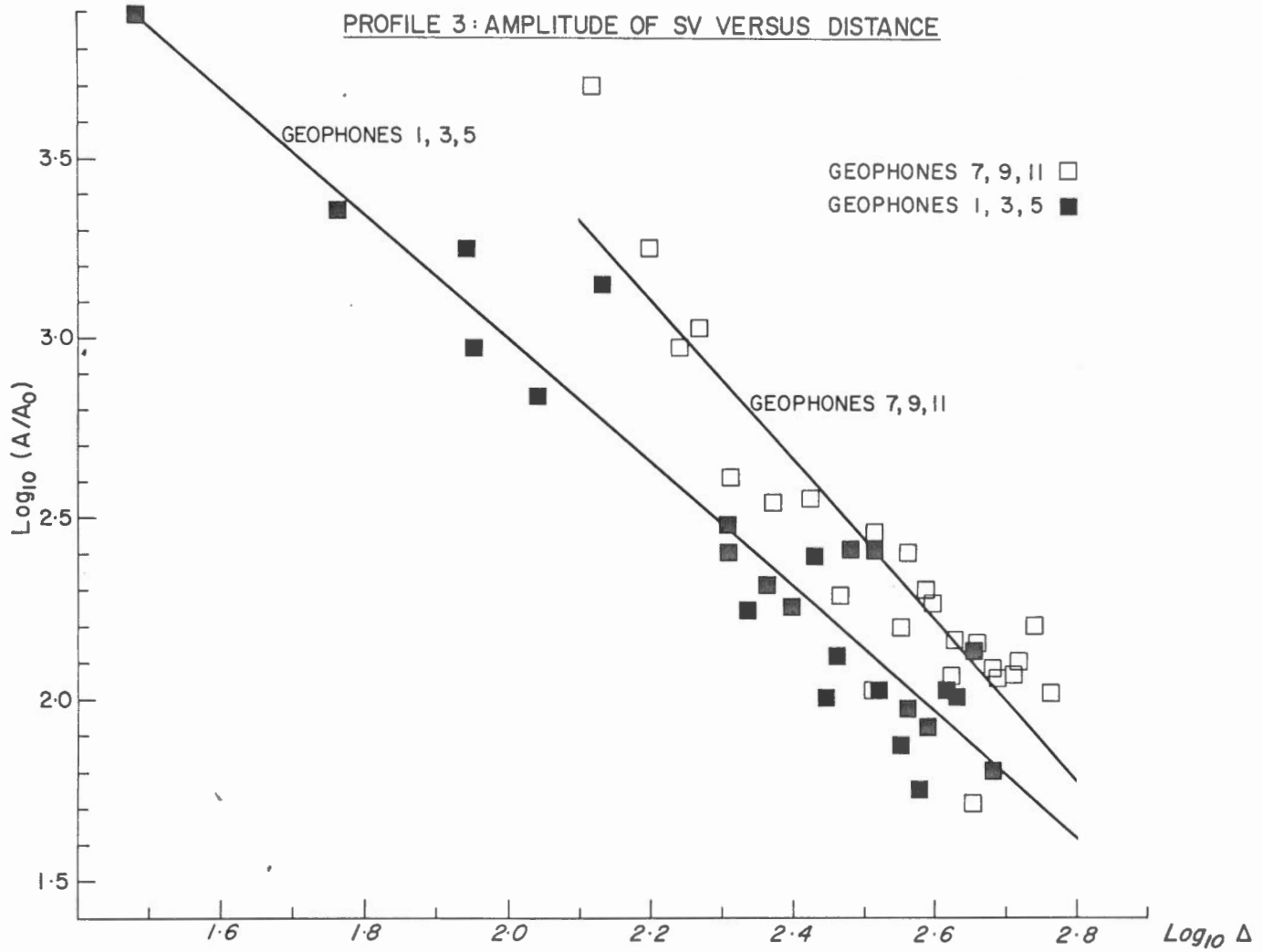
PROFILE 3 : AMPLITUDE OF SV VERSUS DISTANCE
GEOPHONES 1, 3, 5
GEOPHONES 7, 9, 11 □
GEOPHONES 1, 3, 5 ■
GEOPHONES 7, 9, 11
3·5
3·0
2·5
2·0
1·5
Log10 (A/A0)
1·6
1·8
2·0
2·2
2·4
2·6
2·8
Log10 Δ

Fig. 8

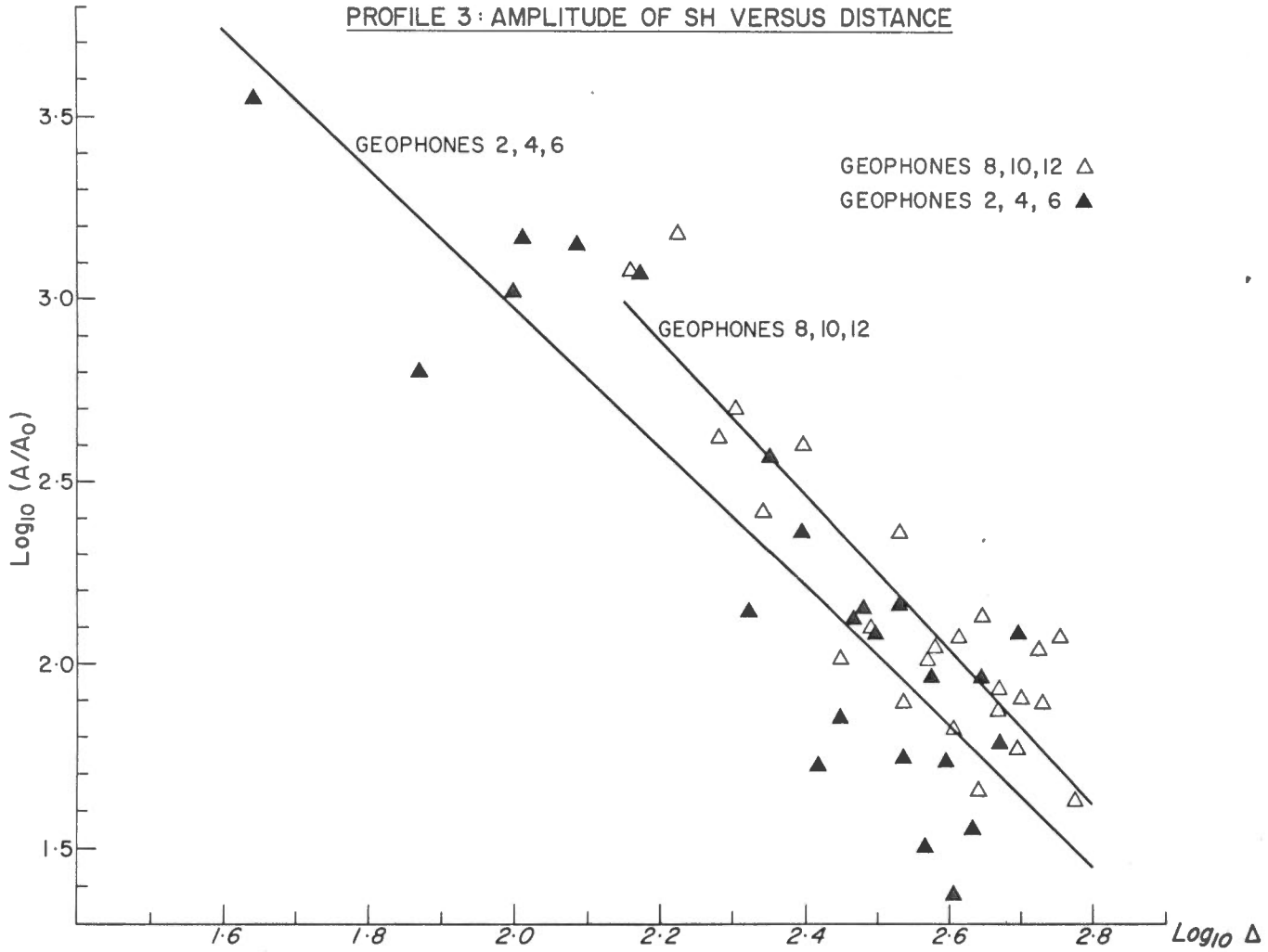
PROFILE 3: AMPLITUDE OF SH VERSUS DISTANCE
GEOPHONES 2, 4, 6
GEOPHONES 8, 10, 12 △
GEOPHONES 2, 4, 6 ▲
GEOPHONES 8, 10, 12
Log10 (A/A0)
3·5
3·0
2·5
2·0
1·5
1·6
1·8
2·0
2·2
2·4
2·6
2·8
Log10 Δ

FIG 9

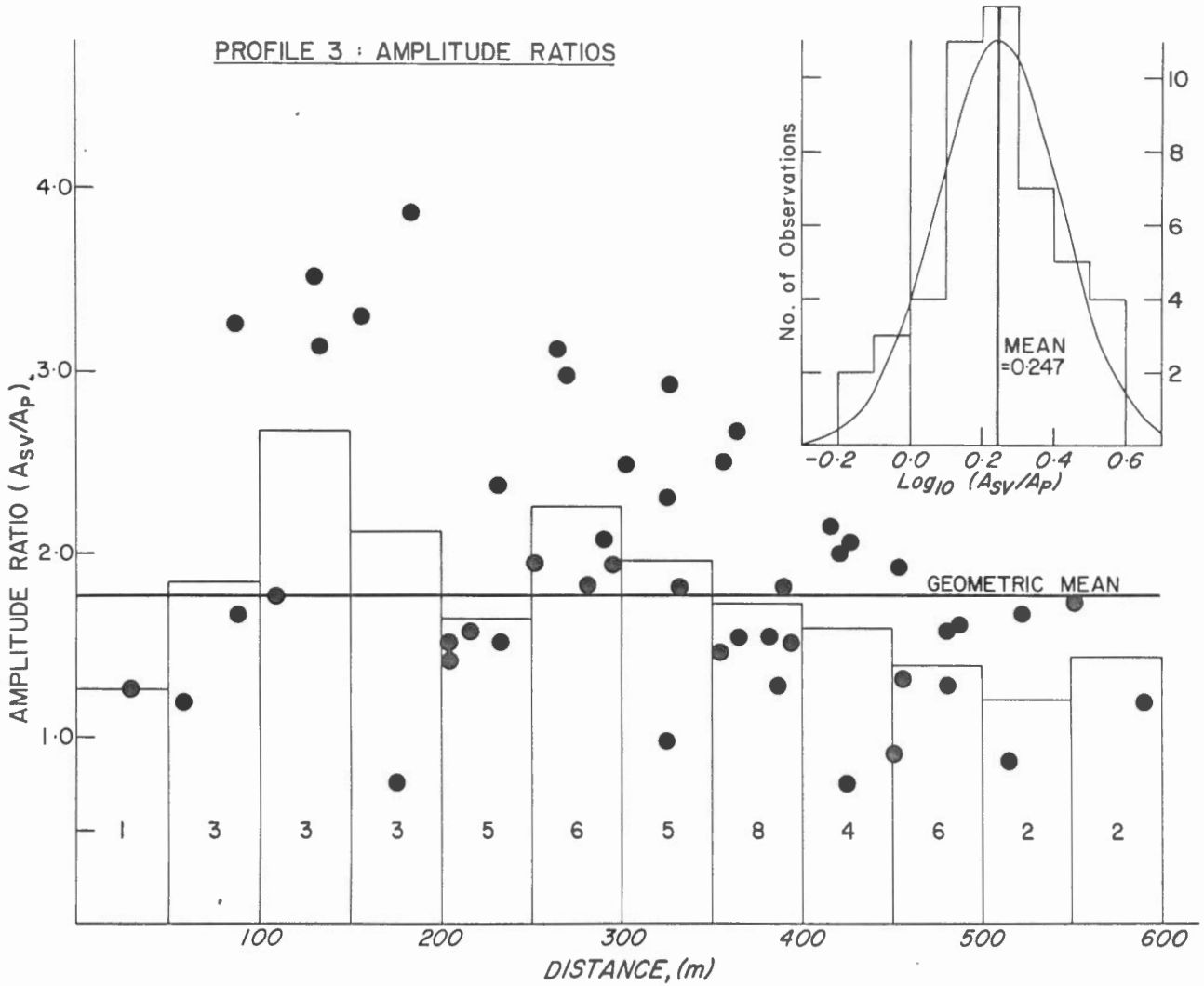
PROFILE 3 : AMPLITUDE RATIOS
AMPLITUDE RATIO (A_{SV}/A_P)
4·0
3·0
2·0
1·0
GEOMETRIC MEAN
1 3 3 3 5 6 5 8 4 6 2 2
100 200 300 400 500 600
DISTANCE, (m)
No. of Observations
10 8 6 4 2
MEAN
=0·247
-0·2 0·0 0·2 0·4 0·6
Log_{10} (A_{SV}/A_P)

Fig. 10

AMPLITUDE RATIOS : A_R/A_V ; A_L/A_V PROFILE 3

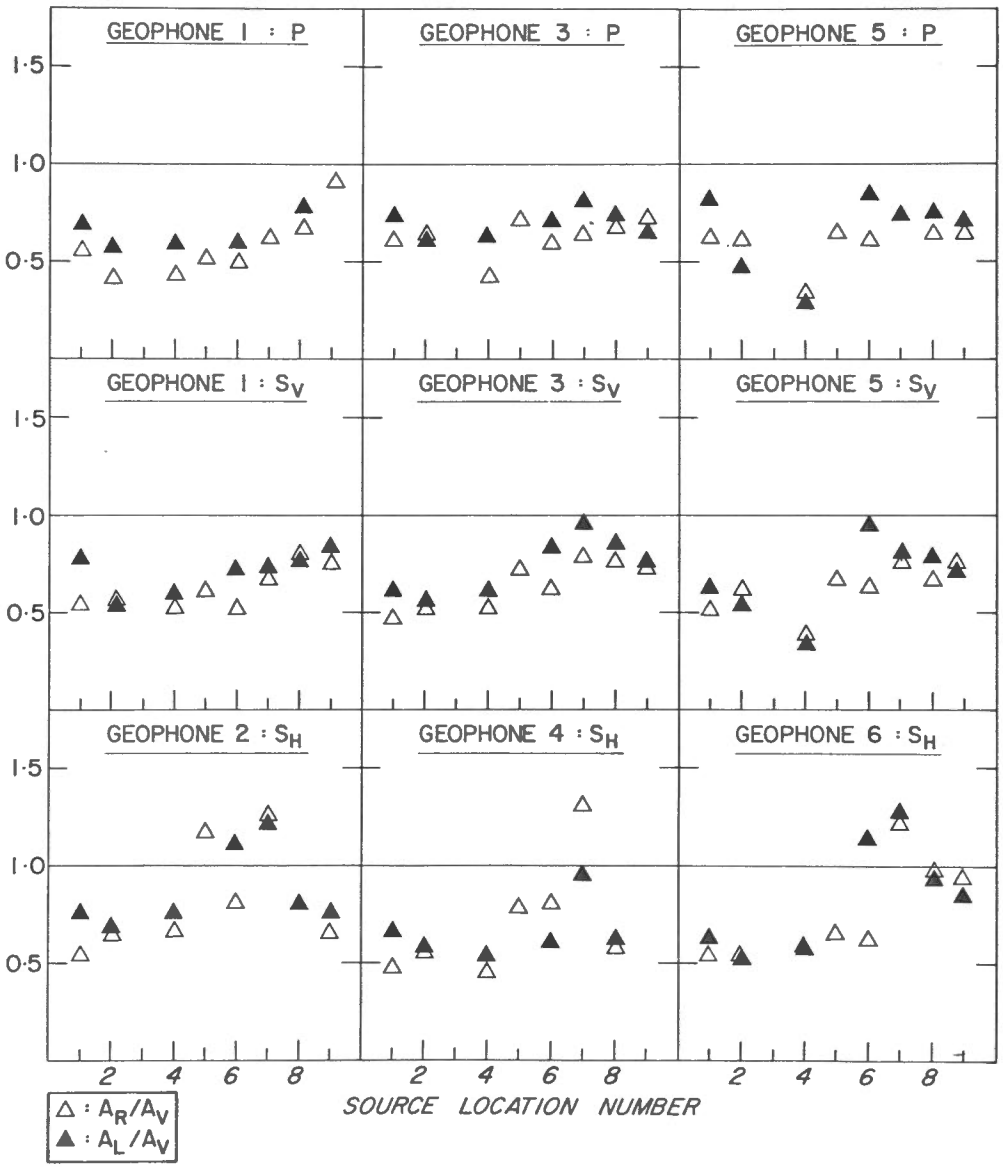

FIG. 11

AMPLITUDE RATIOS : A_R/A_V ; A_L/A_V PROFILE 3

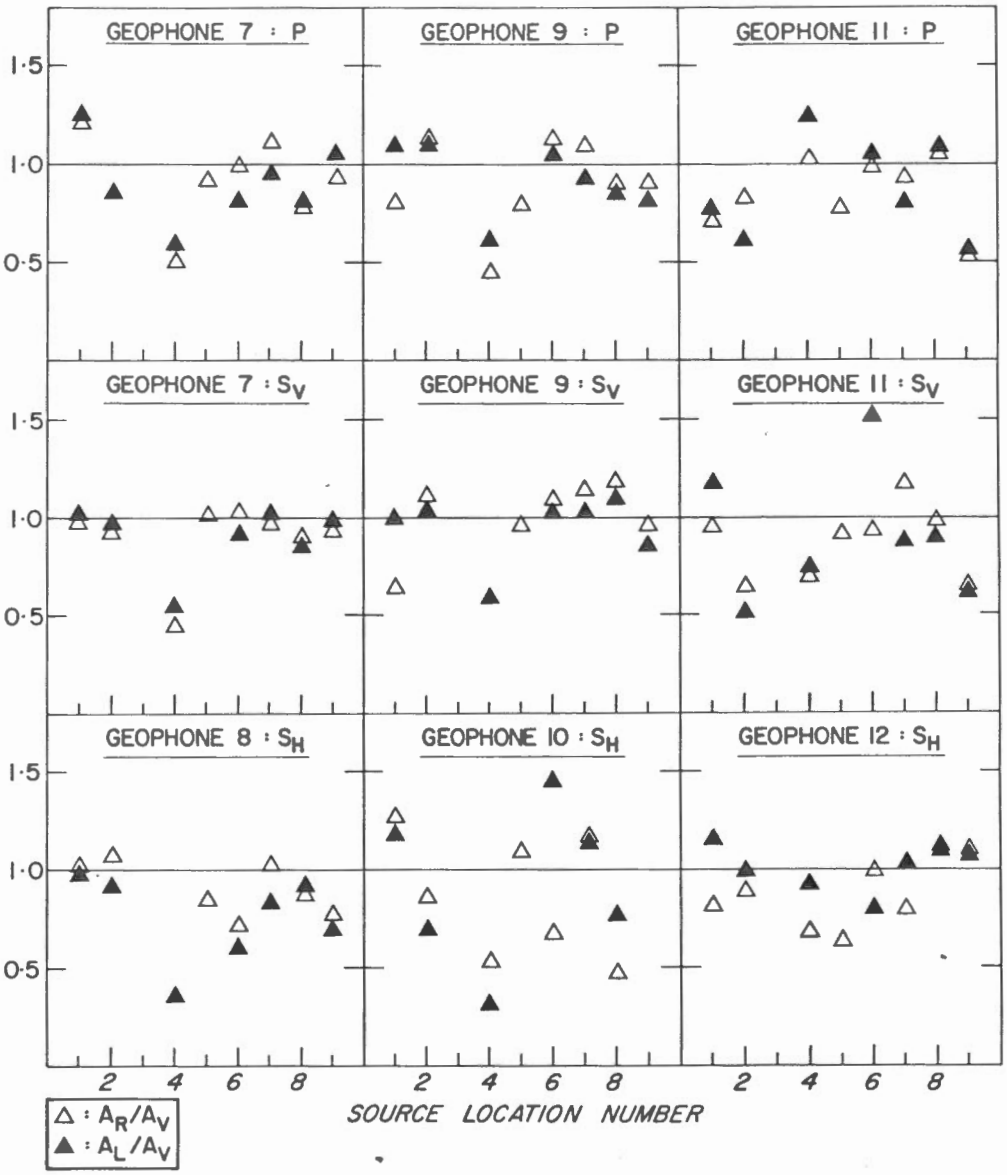

FIG. 12